REPORT DOCUMENTATION PAGE

Form Approved
OMB No. 0704-0188

1. REPORT DATE *(DD-MM-YYYY)*	**2. REPORT TYPE**	**3. DATES COVERED** *(From - To)*
26-02-2009	Journal Article	

4. TITLE AND SUBTITLE

Comparison of X-Ray Micro-Tomography Measurements of Densities and Porosity to Traditional Techniques for Carbon-Carbon Composites

5a. CONTRACT NUMBER

5b. GRANT NUMBER

5c. PROGRAM ELEMENT NUMBER

6. AUTHOR(S)
Erik Weber, Marietta Fernandez, Wesley Hoffman (AFRL/RZSM); Phillip Wapner (ERC)

5d. PROJECT NUMBER

5e. TASK NUMBER

5f. WORK UNIT NUMBER
33SP078H

7. PERFORMING ORGANIZATION NAME(S) AND ADDRESS(ES)

Air Force Research Laboratory (AFMC)
AFRL/RZSM
9 Antares Road
Edwards AFB CA 93524-7401

8. PERFORMING ORGANIZATION REPORT NUMBER

AFRL-RZ-ED-JA-2009-064

9. SPONSORING / MONITORING AGENCY NAME(S) AND ADDRESS(ES)

Air Force Research Laboratory (AFMC)
AFRL/RZS
5 Pollux Drive
Edwards AFB CA 93524-70448

10. SPONSOR/MONITOR'S ACRONYM(S)

11. SPONSOR/MONITOR'S NUMBER(S)
AFRL-RZ-ED-JA-2009-064

12. DISTRIBUTION / AVAILABILITY STATEMENT

Approved for public release; distribution unlimited (PA #09085).

13. SUPPLEMENTARY NOTES
For publication in "Carbon."

14. ABSTRACT

The porosity in carbonaceous materials affects many of their properties. For this reason, the characterization of this porosity is very important. Many diverse techniques have been utilized to characterize the pores in carbon materials. Some of these techniques along with the use of X-ray micro-computed tomography (μCT) have been utilized in this study to provide significant insight into the pore structure of carbon-carbon composites. μCT is not only capable of providing information on the size, shape, and distribution of both open and closed pores in 3-dimensions but in conjunction with mercury porosimetry, it is also able to explain artifacts in the samples.

15. SUBJECT TERMS

16. SECURITY CLASSIFICATION OF:			**17. LIMITATION OF ABSTRACT**	**18. NUMBER OF PAGES**	**19a. NAME OF RESPONSIBLE PERSON**
					Dr. Wesley Hoffman
a. REPORT	**b. ABSTRACT**	**c. THIS PAGE**	SAR	38	**19b. TELEPHONE NUMBER** *(include area code)*
Unclassified	**Unclassified**	**Unclassified**			N/A

Comparison of X-Ray Micro-Tomography Measurements of Densities and Porosity to Traditional Techniques for Carbon-Carbon Composites

E. Weber [a], M. Fernandez [a], P. Wapner [b], W. Hoffman [a,*]

[a] Air Force Research Laboratory, Edwards AFB, CA 93524 United States
[b] ERC, Inc, Edwards AFB, CA 93524 United States

Abstract

The porosity in carbonaceous materials affects many of their properties. For this reason, the characterization of this porosity is very important. Many diverse techniques have been utilized to characterize the pores in carbon materials. Some of these techniques along with the use of X-ray micro-computed tomography (μCT) have been utilized in this study to provide significant insight into the pore structure of carbon-carbon composites. μCT is not only capable of providing information on the size, shape, and distribution of both open and closed pores in 3-dimensions but in conjunction with mercury porosimetry, it is also able to explain artifacts in the samples.

1. Introduction

The characterization of porosity in carbonaceous materials is very important in numerous diverse applications. Depending on the intended application, this porosity can be either very beneficial or detrimental.

For example, in the fields of adsorption, absorption, capacitance, gas storage, and medical applications porosity is desired and should be maximized. Thus, the micropore structure of activated carbons [1] contributes to their extensive use in numerous varied fields that involve purification of toxins, bacteria, chemicals, and odors. The more precise ultra-micropore (<0.7 nm) structure of carbon molecular sieves [2,3] makes them very useful for gas separation while the micropore volume makes

* Corresponding author. Fax: 1-661-275-5073.
E-mail address: wesley.hoffman@us.af.mil (W Hoffman).

carbons useful for electrochemical capacitors [4]. In the medical field, porosity in carbon is used for the controlled release of drugs [5] as well as in implants where the porosity accelerates the growth of a biological connective-tissue film around the implant [6,7]. In addition, porosity plays a significant role, for methane [8] and hydrogen [9] storage in carbonaceous materials as well as in the interaction of carbon black [10] with matrixes in the reinforcement of elastomers.

In applications where mechanical properties are needed, porosity should be minimized or the distribution at least controlled. Thus, as might be anticipated, the porosity in carbon-carbon (C-C) composites negatively affects the tensile [11] and compressive [12] strength as well as the elastic constants [13] and the anisotropy factor [14]. In addition, in nuclear applications, stability to irradiation [15] increased with an increase in the concentration of large pores (10-1000 nm in diameter) as well as a decrease in the concentration of small pores (1-10 nm in diameter).

Reactivity of carbons increases with surface area and more particularly active surface area [16], which is the portion of the total surface area that is reactive for a particular molecule. In applications where reactivity is desired, for example, in uses such as electrodes in double-layer capacitors [17], Li/O_2 batteries [18], prismatic lithium thionyl chloride ($Li/SOCl_2$) batteries [19], fuels cells, and in electrochemical cells, porosity is beneficial and the goal is to maximize the porosity resulting in an increase in the surface area. In applications where reactions produce deleterious results such as swelling, corrosion, and oxidation, porosity should be minimized. Therefore, in contrast to other electrode applications, when carbon cathodes are employed in an aluminum reduction cell [20] porosity should be minimized because it allows the penetration of different electrolyte components, particularly sodium fluoride. This results in swelling of the cathode over time generating high stresses on cathode shell, which reduces cell life. Also, in many carbons and particularly in C-C composites, porosity is minimized to reduce mass-loss [21,22] and thus improve high temperature performance in oxidizing environments.

In many other situations, porosity can also be beneficial or detrimental depending on the application. Thus, as just mentioned in the high temperature use of C-C composites, gas phase reactions are detrimental. In contrast, if gasification of carbon is the goal, porosity is beneficial. Since the thermal conductivity and coefficient of thermal expansion of carbon fiber reinforced composite materials are both dependent on fiber, matrix, and porosity volume fractions [23,24] these parameters can be increased or decreased by varying the porosity of a sample. Porosity is also important in the use of carbon as a catalyst and catalyst support [25] and should be tailored for the particular application. Finally, it should be mentioned that, where porosity is desired, a particular distribution is usually preferred or required. Thus, it is necessary to characterize pore size distributions as well as the total porosity.

There are many techniques utilized to characterize the total porosity and the distribution of porosity in a sample. All the techniques have shortcomings and no one method can characterize the entire range of pore size distribution. Because of these facts, several techniques [26, 27] are usually used to characterize any sample.

Techniques to characterize ultra-micropore (<0.7 nm) distribution include adsorption and desorption of gases using the Dubinin-Radushkevitch (D-R) equation, scanning tunneling microscopy (STM), microflow calorimetry, small angle x-ray scattering (SAXS), and small angle neutron scattering (SANS). For micropores, mesopores, and macropores (<200 nm), adsorption and desorption of gases analyzed by the Brunauer, Emmett, and Teller (BET) equation, along with SAXS, SANS, and STM are employed for pore size distribution.

Microflow calorimetry either makes use of probe molecules of precise dimensions [4,28] or on thermoporometry [29], which is based on a property of liquids in pores. That is, their melting point is dependent upon pore diameter so that a pore size distribution versus pore diameters can be obtained. The

adsorption and desorption of gases [30,31] is analyzed by either the BET equation [32] or the D-R equation [33]. Using the BET equation, nitrogen, argon, and krypton are employed while for the D-R equation CO_2 is usually used. With the adsorption techniques, certain assumption concerning pore shape (cylindrical [34] or slit-shaped [35,36]) are required for analysis and the maximum pore size that can be characterized is 60 nm.

Both SAX and SANS [37,38] provide information similar to each other as well as to that provided by the BET adsorption technique concerning the low-end range (up to 200 nm) of porosity in a carbon sample. These techniques are also able to provide quantitative information on the geometry of transitional pores. Some major advantages of both scattering as well as adsorption techniques are that they are non-destructive, non- intrusive, and do not require sample preparation. Additional advantages for SAXS [39,40] are that the x-ray source is readily available and the source can be mounted on an experiment to record *in situ* porosity changes while an experiment is running. Although SANS [41-43] measurements require a source of neutrons, which are not readily available, this technique offers the additional advantage that with contrast matching (SANS-CM) it is sensitive to both 'closed' (inaccessible) and 'open' (accessible) pores. That is, the technique can estimate closed porosity utilizing contrast matching in which the accessible porosity is filled with a suitable liquid for contrast.

To view individual pore size and shape at these dimensions, transmission electron microscopy [44] and STM [27] are used. However, it should be noted that the short-comings of these technique as with all image analysis techniques, such as scanning electron microscopy (SEM) and optical microscopy, are that the images are in the form of a 2-dimensional cross-sections and only a small part of the sample can be examined at one time meaning that it is difficult to get a statistically valid result.

To ascertain the total porosity and pore size distribution above 3 nm, mercury porosimetry [45,46] is usually chosen and most often employed [47-51] because it is useful to characterize the entire range of

the pore size distribution above this minimum value. As with all methods, this technique has some limitation, such as, the possibility of damaging the pore walls [52,53] with the high pressure (414 MPa) which skews the results, not knowing the exact contact angle of mercury with the pore walls, being limited to a small sample size, and rendering the sample toxic and unsuitable for future processing or testing. The SEM [54,55] and STM [27,56] are also useful in this range and are frequently used along with porosimetry to characterize pore size distribution.

For samples with much larger pores, X–rays can be used to image pore size and shape in carbonaceous samples. The first images [57] were obtained by transmission-computed tomography that had a resolution close to 1 mm. Recently, X-ray micro-computed tomography (μCT) has become commercially available with some instruments having sub-micron resolution that is useful for nondestructively examining a sample in 3-dimensions (3D). These instruments have been used in various material science applications [58] for evaluation of porous structures [59], and morphology changes in stone [60] and cellular ceramics [61] to name just a few. Various carbon-based materials have also been examined using μCT in applications, such as the determination of the effects of graphite oxidation [62,63], the relationship between the density and mechanical properties of C-C composites [64], the porosity effects on the mechanical properties of graphite [65], and quantification of other properties [61].

As a final point, there are several techniques that can provide a global measure of porosity. Ultrasonic techniques [66-68] rely on the transmission of acoustic waves through a sample while gas pycnometry [52,69,70] provides a density value based on intrusion of a gas, such as helium, into the pore structure. This intrusion density is compared to the bulk density to give a value of open porosity. Water in conjunction with vacuum [71] or boiling [72] are also employed to intrude into the pore

structure to characterize it. Lastly, other liquids are used in a density gradient column [73-75] employing a sink-float technique in an attempt to get an accurate value for the density.

Realizing the shortcomings of each technique mentioned above to characterize pore size distribution of a sample as well as the unique advantages of μCT in viewing the pore structure in 3D, the decision was made to compare the results of various techniques on a rather large sampling of different C-C composite samples to grasp the value of μCT.

C-C composites were chosen as samples because of their superior high temperature mechanical and frictional properties and because they have a wide range of porosity distributions. In addition, since the μCT is non-destructive, it allows density measurements through successive densification and heat-treatment steps on the same sample. This capability permits directly quantifying the affects of each of the processing steps and the perturbation of processing parameters. μCT also provides a method to determine the closed porosity of a representative sized sample of a C-C composite. However, it should be noted that depending on the samples, sample size, and type of instrument chosen, there are limitations to μCT analysis due to sub-pixel resolution, and processing time.

2. Materials and Methods

2.1 Materials

To provide a range of porosities and densities, composite specimens were selected from a wide range of samples formed from different fiber preforms by a number of different processing techniques. Undensified fiber preform samples were not analyzed due to the difficulty with a number of different test methods including the μCT. Specifics of each sample can be found in Table 1. Felt samples 1-28 were produced from a felted preform subjected to either 1 or 2 densification cycles employing either the *In Situ* Densification Process [76] or AR mesophase pitch supplied by Mitsubishi Oil with different processing conditions. The felt samples were cut to size before densification while the rest of the

samples were cut out of larger densified samples. PPMC samples were produced from a fiber layup and densified with a standard pitch process. Some of these samples were then further densified with the *In Situ* process. In addition, some had heat treatments at different points in the processing. The CF samples were produced from a chopped fiber preform, which was rigidized with phenolic resin and then densified with the *In Situ* process. The samples whose designations start with 2D and 3D were produced commercially from the preform and by the process described.

Table 1

Sample Name	Sample Information
2D A 1	2D Phenolic pre-preg then 1 cycle coal tar pitch
2D B 1	2D; Phenolic pre-preg; 1 cycle Pitch
2D B 2	2D; Phenolic pre-preg; 1 cycle Pitch
3D A 1	3D Radially-pierced cylindrical weave densified with Petroleum Pitch
3D B 1	3D pierced fabric densified by chemical vapor deposition
CF 1	Chopped fiber layup; 1 cycle phenolic; 1 cycle *In Situ*
CF 2	Chopped fiber layup; 1 cycle phenolic; 1 cycle *In Situ*
CF 3	Chopped fiber layup; 1 cycle phenolic; 1 cycle *In Situ*
CF 4	Chopped fiber layup; 1 cycle phenolic; 1 cycle *In Situ*
CF 5	Chopped fiber layup; 1 cycle phenolic; 1 cycle *In Situ*
CF 6	Chopped fiber layup; 1 cycle phenolic; 1 cycle *In Situ*
CF 7	Chopped fiber layup; 1 cycle phenolic; 1 cycle *In Situ*
CF 8	Chopped fiber layup; 1 cycle phenolic; 1 cycle *In Situ*
Felt 1	Felt preform; 1 cycle *In Situ*; oxidized 10%
Felt 2	Felt preform; 1 cycle AR mesophase
Felt 3	Felt preform; 1 cycle *In Situ*
Felt 4	Felt preform; 1 cycle AR mesophase
Felt 5	Felt preform; 2 cycle *In Situ*
Felt 6	Felt preform; 1 cycle *In Situ*; 1 cycle AR mesophase
Felt 7	Felt preform; 2 cycle *In Situ*
Felt 8	Felt preform; 1 cycle *In Situ*; 1 cycle AR mesophase
Felt 9	Felt preform; 2 cycle *In Situ*
Felt 10	Felt preform; 2 cycle *In Situ*
Felt 11	Felt preform; 1 cycle *In Situ*; 1 cycle AR mesophase
Felt 12	Felt preform; 2 cycle *In Situ*
Felt 13	Felt preform; 2 cycle *In Situ*
Felt 14	Felt preform; 1 cycle *In Situ*
Felt 15	Felt preform; 1 cycle *In Situ*; Oxidized to 7% wt. loss
Felt 16	Felt preform; 1 cycle *In Situ*; 1 cycle AR
Felt 17	Felt preform; 1 cycle *In Situ*; Oxidized 2%
Felt 18	Felt preform; 2 cycle *In Situ*
Felt 19	Felt preform; 1 cycle *In Situ*; Oxidized 11%
Felt 20	Felt preform; 1 cycle *In Situ*; Oxidized 13%
Felt 21	Felt preform; 1 cycle *In Situ*; Oxidized 8%
Felt 22	Felt preform: 1 cycle *In Situ* mesophase: 1724 kPa
Felt 23	Felt preform; 1 cycle AR mesophase
Felt 24	Felt preform; 1 cycle AR mesophase; 1,206 kPa
Felt 25	Felt preform; 1 cycle AR mesophase; 3,447 kPa
Felt 26	Felt preform; 1 cycle AR mesophase; 137 kPa
Felt 27	Felt preform; 1 cycle AR mesophase; 3,447 kPa
Felt 28	Felt preform: 1 cycle *In Situ* mesophase: 1724 kPa
PPMC 1	Chopped fiber layup; 1 cycle pitch
PPMC 2	Chopped fiber layup; 1 cycle pitch; heat-treatment
PPMC 3	Chopped fiber layup; 1 cycle pitch; 1 cycle pitch; heat-treatment
PPMC 4	Chopped fiber layup; 1 cycle pitch; 1 cycle *In Situ*
PPMC 5	Chopped fiber layup; 1 cycle pitch; heat-treatment; 1 cycle *In Situ*
PPMC 6	Chopped fiber layup; 1 cycle pitch; 1 cycle pitch; heat-treatment; 1 cycle *In Situ*
PPMC 7	Chopped fiber layup; 1 cycle pitch; 1 cycle pitch; heat-treatment; 1 cycle *In Situ*
PPMC 8	Chopped fiber layup; 1 cycle pitch; 1 cycle pitch; heat-treatment; 1 cycle *In Situ*

2.2 Preparations of samples

Forty-nine samples were cut into cylinders with a diameter of Ø = 13.8 mm and a length not exceeding 30 mm. A cylinder shape was chosen because it was the best-fit for the μCT scanning, AutoPore Mercury Porosimeter, and Quantachrome Helium Pycnometer sample holders. Samples were oven dried for 24 hours at 110°C before being subjected to each different method of density measurement.

2.3 μCT

A Skyscan 1172 High-Resolutions Micro CT was used for imaging and evaluating forty-nine C-C samples. The tungsten micro-focus x-ray tube was set at 40 kV and 250 μA without a filter. Radiographs of 16.1, 8.0, and 4.0 μm/pixel were acquired from a 4,000×2,096 CCD camera binned for the lower resolutions over 180°. After placing the sample in a nylon clamp holder, the whole sample was scanned in up to six successive horizontal sections controlled by the system software. Typical μCT processing conditions for each resolution can be found in Table 2.

Table 2

	Pixels	Frames Averaged	Rotation Step	Random Movement
16.1 μm	1,000×512	12	0.7°	10
8.0 μm	2,000×1,024	12	0.4°	10
4.0 μm	4,000×2,048	12	0.3°	10

After scanning, the resultant radiographs were reconstructed into numerous 2D slices using a modified Feldkamp cone-beam algorithm [77] and then the horizontal sections were joined. The whole data stack was analyzed using "CTAn" software and a custom analysis algorithm. A summary of the capabilities and steps of the algorithm employed are given in Table 3. This custom algorithm allowed the percentage of open and closed porosity of as well as the bulk density of each sample to be determined. Care had to be taken when the threshold values for each sample were chosen because it significantly affected the results.

Table 3

	Reason	Actions
Manual Operations	Setup of image stack	Determine general the region of interest (ROI) to remove holder and other non-required items Threshold between air and carbon Save binary image stack
Automatic Operations	Basic image processing and Region of Interest (ROI) setup	Open binary image stack Threshold – global – 44 to 255 De-speckle – Sweep in 3D ROI Shrink-wrap – Stretch over 50 pixels in 2D
	Determination of closed porosity	De-speckle – Sweep in 3D De-speckle – Remove broken pores in 3D determined by ROI borders De-speckle – Remove black speckles that are less than 20 voxels Threshold – Global – 0 to 244 3D Analysis
	Determination of open porosity	Reload binary images Threshold – Global – 0 to 244 De-speckle – Sweep in 3D De-speckle – Remove pore in 3D determined by ROI borders De-speckle – Remove black speckles that are less than 20 pixels Threshold – Global – 0 to 244 3D Analysis
	Determination of solid	Reload binary images Threshold – Global – 0 to 244 De-speckle – Sweep in 3D 3D Analysis

2.4 Vacuum Water/2-Propanol Saturation Technique (VWST) and Boiling Water Saturation (BWS)

VWST was carried out generally according to ASTM C830 [71]. A custom-made system was built for the vacuum water/2-propanol saturation technique. In this method, the sample was pulled-out of the oven and the dry weight was determined. The specimen is then placed in an empty flask and evacuated for 30 minutes. Water was then brought in, to totally submerge the sample while keeping it under vacuum. The water was allowed to saturate the specimen for 30 minutes. After 30 minutes the sample while still submerge in water was weighed and the water temperature was determined. The same process and system was used for the sample in 2-propanol.

BWS was carried out according to ASTM C20 [72]. In this method, the sample oven-dry weight was first determined. The sample was then levitated in a beaker and submerged in distilled water. The

distilled water in which the specimen was submerged was boiled for 3 hours and then was left to cool to room temperature for at least 12 hours before determining the weight of the sample in water.

After the μCT scan and the two water density measurements, each sample was cut in two pieces. ($L_1 \approx 18$ mm; $L_2 \approx 13$ mm). The smaller piece (L_2) was used for the pycnometer measurement followed by a sink-float density determination in sodium polytungstate. The larger sample L_1 was used as the mercury porosimeter sample.

2.5 Helium Pycnometer

An UltraPycnometer1000 Version 2.12 from the Quantachrome Corporation was used in this density measurement. This apparatus uses helium gas as the fluid for displacement because helium is the smallest inert molecule.

Before each sample measurement, the system is standardized with two stainless steel spheres of known density. Sample runs consists of 3 consecutive runs with a deviation equal to or less than 0.050% or 10 runs if the required set deviation is not attained.

2.6 Mercury Porosimeter

The principle of mercury porosimetry relies on the non-wetting nature of mercury. This means that if a sample is evacuated and then covered with mercury, the liquid will not intrude into the porosity until sufficient pressure has been supplied. The porosity measurement is made by evacuating the chamber with a sample in it, covering the sample with mercury, and then incrementally pressuring the chamber while measuring the volume intruded into the sample. A significantly low pressure is used to determine the total volume of the sample including both open pores and carbon. This total volume of the sample is also used to determine the bulk density of the sample therefore the choice of the low-pressure value is critical. At each subsequent incremental increase in pressure, the volume of mercury intrusion is measured. The incremental percent porosity for that pressure increment is calculated by dividing the

incremental intrusion volume by the sample initial volume. Each pressure increment is also correlated by a number of assumptions to a range of pore diameters and is reported as the mean of the range of pore diameter (MPD) for that increment. The use of small pressure increments can significantly increase the resolution of the test allowing for closer correlation with the μCT data. At the completion of the porosimetry test, the total porosity is calculated by the dividing the total mercury intrusion volume by the initial volume. The total skeletal density is calculated by taking the initial weight of the sample and dividing it by the quantity of the initial total volume minus the total mercury intrusion volume.

Micromeritic's Auto Pore IV 9520/ 9500 Version 1.07 software was used to determine percent porosity, porosity size, bulk density, and skeletal density of the sample. The weight of the oven-dry sample was first determined and recorded. The penetrometer was then evacuated to pressure less than 7 Pa, followed by filling with mercury at 3,447 Pa in at least 147 incremental intrusion pressures to 275 kPa, using nitrogen gas as the displacing medium. The sample is then loaded into the high-pressure chamber of the Autopore IV system. The high-pressure run was from 276 kPa – 414 MPa in at least 649 increments, using hydraulic oil as the displacing medium. An additional constraint was place on the run that the maximum mercury intrusion of each pressure increment was 0.010 ml/g of sample to maximize the resolution of the run.

2.7 Sink-Float

In this density measurement method, sodium polytungstate solution that has an initial density of 2.89 g/cm^3 was used. Samples were placed in re-sealable vials with a known volume of low-density (1.19 g/cm^3) solution of sodium polytungstate. A known volume of the higher density solution (2.46 g/cm^3) was incrementally added from a burette to vials that contained the samples and each sample was left soaking in the solution until it achieved equilibrium at which point the position of the sample was observed. This procedure was repeated until each sample floated in the liquid for at least 24 hours.

3. Results and Discussion

There are many variables that affect the porosity of C-C composites. Fiber preforms are made from tows of fibers that may contain from 1-60,000 individual fibers. There is obviously intra-tow porosity among the fibers. The tows are placed in the orientation desired for mechanical or thermal properties. This may be a random orientation, is usually orderly in a 1-3 dimensional structure, but can have tows in 4-11 different orientations. The space between the fiber bundles is called a pocket and the size of this pocket and thus the porosity will vary with the size of the tows as well as the spacing of the tows from one another. Finally, the porosity in the densified preform will be dependent on the extent, uniformity, and efficiency of the densification process. Obviously, what constitutes a representative C-C samples will depend on several of these variables. Testing of representative samples of C-C is important when looking at both open and closed porosity since they are very dependent of the sample and its size. The smaller the sample, for example, the lower the likelihood there will be closed porosity.

As will be seen, the various techniques employed generally give very similar results. The choice of technique for a particular application will depend on the equipment available and the advantages and disadvantages of each technique. For example, the μCT and the mercury porosimeter provide the most information on each sample but are limited in sample size and minimum pore size that can be measured. In addition, the process of making a mercury porosimetry measurement destroys the sample. On the other hand, all the immersion and displacement techniques are much simpler and easier to use. With the exception of the helium pycnometry, all these immersion and displacement techniques are also able to evaluate much larger samples that provide a more representative value. However, it should be noted that the sink-float technique has some unique issues for porous samples that will be described below.

3.1 Skeletal Density

The results for the six different skeletal density measurements can be found in Table 4. With the exception of the sink/float method, all the densities measurements were very close to each other. The sink/float results were not included in the average and standard deviation for each sample due to the large deviation from the other techniques. The results show that on average, the porosimeter gives the highest density and the vacuum immersion has the lowest. The average difference between the maximum and minimum value for a samples is 0.075 g/cm^3 or 4.0% of reading. The difference in techniques appears to be the minimum pore size that the testing medium reaches.

The sink/float test method has four major problems associated with it. First, the sink/float method relies on a sodium polytungstate solution to completely fill the smallest pores of the composite without any outside driving force such as vacuum, pressure, or heat. Secondly, it assumes a homogeneous mixture throughout the pore structure after each high-density solution aliquot is added. Thirdly, the sodium polytungstate solution easily changes density due to evaporation of the water. Finally, the sample is contaminated with sodium polytungstate after the measurement and cannot be reused. The combination of the first three factors leads to unreliable and inaccurate results, and should not be used on materials with significant porosity.

Table 4

Sample Name	Vacuum Immersion	Boiling Immersion	2-Propanol Vacuum Immersion	Helium Pycnometer	Mercury Porosimeter	Average	Standard Deviation	Sink/ Float
2D A 1	1.619	1.609	1.623	1.616	1.639	1.621	0.011	-
3D A 1	2.036	2.044	2.082	2.063	2.105	2.066	0.028	-
3D B 1	2.038	2.034	2.099	2.098	2.151	2.084	0.049	-
2D B 1	1.683	1.683	1.685	1.696	1.710	1.691	0.012	-
2D B 2	1.777	1.772	1.769	1.780	1.785	1.777	0.006	-
CF 1	1.970	1.994	1.916	2.155	1.929	1.993	0.096	-
CF 2	1.959	2.026	1.917	2.140	-	2.010	0.097	1.20
CF 3	2.064	2.084	2.096	2.103	2.422	2.154	0.151	-
CF 4	2.082	2.089	2.078	2.102	-	2.088	0.010	1.20
CF 5	1.755	1.753	1.640	-	1.975	1.781	0.140	-
CF 6	1.757	1.767	1.648	-	-	1.724	0.066	1.20
CF 7	2.008	1.984	2.037	2.016	2.112	2.031	0.049	-
CF 8	2.007	1.993	2.036	2.022	-	2.015	0.018	1.52
Felt 1	1.857	1.858	1.859	1.860	1.853	1.857	0.003	1.72
Felt 2	1.429	1.431	1.436	1.448	1.471	1.443	0.017	1.40
Felt 3	1.830	1.840	1.838	1.838	1.846	1.838	0.006	1.46
Felt 4	1.420	1.423	1.430	1.438	1.464	1.435	0.018	1.31
Felt 5	1.877	1.885	1.894	1.873	1.891	1.884	0.009	1.60
Felt 6	1.692	1.700	1.713	1.706	1.720	1.706	0.011	1.59
Felt 7	1.904	1.899	1.920	1.897	1.906	1.905	0.009	1.76
Felt 8	1.699	1.708	1.716	1.724	1.728	1.715	0.011	1.61
Felt 9	1.877	1.889	1.898	1.877	1.906	1.889	0.013	1.55
Felt 10	1.879	1.886	1.897	1.878	1.836	1.875	0.023	1.58
Felt 11	1.697	1.698	1.714	1.708	1.711	1.706	0.008	1.59
Felt 12	1.868	1.874	1.869	1.867	1.892	1.874	0.010	1.66
Felt 13	1.863	1.870	1.861	1.872	2.039	1.901	0.077	1.64
Felt 14	1.840	1.847	1.841	1.845	1.936	1.862	0.042	1.38
Felt 15	1.877	1.878	1.878	1.877	1.824	1.867	0.024	-
Felt 16	1.711	1.718	1.722	1.741	1.764	1.731	0.021	1.54
Felt 17	1.880	1.883	1.881	1.880	1.857	1.876	0.011	1.56
Felt 18	1.875	1.880	1.874	1.879	1.886	1.879	0.005	1.66
Felt 19	1.873	1.890	1.860	1.889	1.873	1.877	0.013	1.60
Felt 20	1.872	1.887	1.866	1.885	1.908	1.884	0.016	1.64
Felt 21	1.883	1.884	1.893	1.876	1.915	1.890	0.015	1.71
Felt 22	1.830	1.841	1.832	1.838	1.854	1.839	0.009	1.40
Felt 23	1.439	1.439	1.440	1.458	1.494	1.454	0.024	1.34
Felt 24	1.427	1.427	1.428	1.446	1.440	1.434	0.009	1.46
Felt 25	1.431	1.432	1.434	1.452	1.443	1.439	0.009	1.43
Felt 26	1.431	1.432	1.432	1.454	1.450	1.440	0.011	1.35
Felt 27	1.440	1.441	1.443	1.468	1.444	1.447	0.012	1.41
Felt 28	1.590	1.606	1.561	1.602	1.629	1.598	0.025	-
PPMC 1	1.806	1.868	1.821	1.850	1.859	1.841	0.026	-
PPMC 2	1.967	1.993	2.011	2.007	2.065	2.008	0.036	-
PPMC 3	1.980	2.004	2.017	2.015	2.105	2.024	0.047	-
PPMC 4	1.797	1.806	1.798	1.801	1.879	1.816	0.035	-
PPMC 5	1.929	1.974	2.006	1.970	2.061	1.988	0.049	-
PPMC 6	1.919	1.988	1.938	1.994	2.081	1.984	0.063	-
PPMC 7	1.905	1.892	1.890	1.923	2.068	1.936	0.075	-
PPMC 8	1.901	1.907	1.887	1.926	-	1.905	0.016	1.71

3.2 Bulk Density

The results for the four different bulk density measurements can be found in Table 5. All of the density measurements were very close with an average per sample standard deviation of 0.011 g/cm^3. The average difference between the maximum and minimum value for a samples is 0.018 g/cm^3 or 1.8% of the average reading. It appears that varying the resolution of the μCT does not significantly affect the results. The geometric bulk density is not included in this table due to the irregular shapes of many of the samples.

The advantages of the μCT technique are that you can measure larger samples and the same sample after multiple different processing steps. Thus, although this technique provides pore size information similar to the porosimeter it has the advantage over the porosimeter that it does not contaminate the sample so that it cannot be reused. In addition, for the given resolutions, samples of approximately 13 mm in diameter by 500 mm tall can be analyzed. This is in contrast to the porosimeter, which is limited to a sample size of 25 mm x 25 mm. The primary drawback for the μCT is that it is very time consuming. Typically, 17 hours of machine operation are required for scanning, reconstruction, and analysis with 1 hr of operator's time for low-resolution scans and 56 hr of machine operation and 2 hr of operator's time for medium-resolution scans of a sample approximately 13 mm by 30 mm. As with the porosimeter, the choice of starting parameters (in this case the choice of shrink-wrap region of interest spanning) affects the bulk density result.

Table 5

Sample Name	Mercury Porosimeter	µCT Low 16.1 µm	µCT Med 8.0 µm	µCT Hi 4.0 µm
3D B 1	1.922	1.935	1.932	-
2D B 1	1.399	1.400	1.403	-
2D B 2	1.469	1.495	1.499	-
2D A 1	1.022	1.036	1.034	-
3D A 1	1.881	1.903	1.895	1.898
CF 1	0.503	0.729	0.716	-
CF 3	0.794	0.783	0.779	0.766
CF 5	0.572	0.576	-	-
CF 7	1.391	1.374	-	-
Felt 1	1.036	1.019	-	-
Felt 3	1.139	1.132	-	-
Felt 4	1.309	1.315	-	-
Felt 5	1.467	1.464	-	-
Felt 6	1.528	1.525	-	-
Felt 7	1.372	1.364	-	-
Felt 8	1.518	1.527	-	-
Felt 9	1.471	1.461	-	-
Felt 10	1.455	1.458	-	-
Felt 11	1.538	1.539	-	-
Felt 12	1.508	1.489	-	-
Felt 13	1.411	1.414	-	-
Felt 14	1.226	1.209	-	-
Felt 19	1.446	1.424	-	-
Felt 20	1.432	1.422	-	-
Felt 21	1.146	1.124	-	-
Felt 22	1.222	1.210	-	-
Felt 23	1.302	1.289	-	-
Felt 26	1.303	1.278	-	-
Felt 27	1.284	1.290	1.292	-
Felt 28	1.334	1.303	1.307	-
PPMC 1	1.556	1.572	1.567	-
PPMC 2	1.574	1.581	1.575	-
PPMC 3	1.563	1.565	1.562	-
PPMC 4	1.538	1.543	1.531	-
PPMC 5	1.610	1.601	1.596	-
PPMC 6	1.640	1.649	1.646	-
PPMC 7	1.676	1.675	-	-

3.3 Open porosity

The results for the open porosity analysis can be found in Table 6, Table 7, and Table 8. The porosimeter results were compared to the µCT results at three different resolutions (16.1, 8.0, and 4.0 µm). In these tables, the column of Porosimeter percent open-porosity encompasses the total open porosity down to a MPD of 3 nm, which is the ultimate resolution of the instrument. In order to compare the open porosity values from the two instruments, it is necessary to limit the value of the open porosity determined by the porosimeter to the pores equal to or greater than the resolution of the specific µCT scan. This is done by truncating the porosimeter data at a MPD close to the µCT scan resolution. The column, Porosimeter Percent Open Porosity at MPD is the amount of open porosity measured down to the given MPD. The data is provided so a direct comparison can be made between the µCT and porosimeter results. The number of layers analyzed is provided to give an idea of the size of µCT data set analyzed.

The porosimeter results (Table 6, column 2) show that the percent open porosity is much larger than any of the μCT results. This is because the porosimeter measures pores down to 3 nm compared to approximate 4.0, 8.0, or 16.1 μm for the μCT. With samples that were analyzed by both μCT and porosimeter, the μCT results were on average 49.3% lower but ranged from 5.6% to 96.73% lower. This large distribution depended on the size as well as the shape of the pores. A significant advantage of the porosimeter is it gives a distribution of percent porosity with respect to pore size. An example of a distribution can be seen in Figure 1. Figure 1 depicts the total amount of open porosity greater than or equal to a given mean pore diameter.

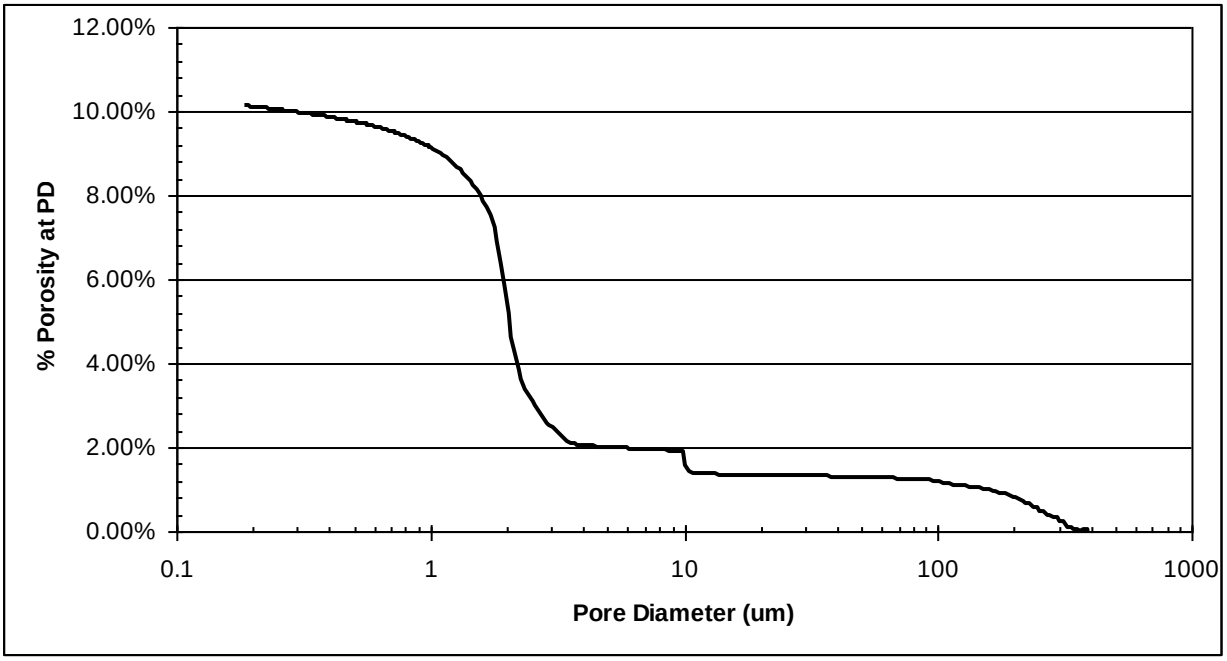

Figure 1

As just stated, when compared to the porosimeter at full resolution (Table 6, column 2), the μCT's results are very low, but when compared at similar resolution (Table 6, column 3; Table 7 and Table 8, column 2), results are much more consistent. The percent of open porosity greater than or equal to MPD measured by the porosimeter is greater than μCT measurements 50% of the time with an average absolute deviation of 3.6% porosity with μCT resolution of 16.1 μm. The percent of open porosity

greater than or equal to MPD measured by the porosimeter is greater than μCT measurement 39% of the time with an average absolute deviation of 6.1% porosity with μCT resolution of 8 μm. The percent of open porosity greater than or equal to MPD measured by the porosimeter is greater than μCT measurement 50% of the time with an average absolute deviation of 23.5% porosity with μCT resolution of 4.0 μm.

The μCT provides a nondestructive method for determining percent open porosity fairly accurately but is significantly limited by the resolution. Increasing the resolution of the μCT scan allows for the imaging of smaller pore diameters while requiring a significantly greater amount of time for data acquisition and manipulation. The ability to determine open porosity non-destructively allows a single sample to be evaluated though a number of processing steps such as densifications and heat treatment. The μCT currently does not allow for the creation of a distribution of open pore size, but it does allow for visualization of the sample either in 2D slices or a 3D representation of the open porosity (Figure 2). The 2D visualization gives the ability to see the shape and distribution of porosity non-destructively throughout the sample with much less effort than slicing and imaging [57] as has been done previously.

The 3D visualization software provides the capability to see the pore shape and distribution in 3D. Figure 2 shows both open and closed porosity in sample PPMC 2. This image is looking down on to the top of the model and is a selection of 150 slices from the middle of the sample. The blue objects are closed pores, the gray objects are open pores, and the white regions signify that there is only carbon and there are no pores in any of the layers at that location. Both the blue and gray pores are 80% transparent so you can see the general amount of stacked-up porosity at each location by the intensity of the color. This image provides an extremely insightful view of the sample's porosity in three dimensions allowing the visualization of the amount, shape, and distribution of open and closed porosity. The model could be

rotated or tilted in any orientation in 3D and anaglyphic glasses allow one to see the perspective in depth.

Although Figure 2 provides very useful data on the quantity and distribution of porosity through many slices of the sample, it is difficult to see the distribution of the porosity through the sample without rotating it. Thus, a portion of the data in Figure 2, marked by the dark region in the inset of Figure 3, is isolated and displayed in Figure 3. In this image, only the closed porosity data for a small volume through the 150 slices of the sample is presented. It is obvious that it is much easier to see the shape of the closed porosity in this volume and to see that it is only a small percentage of the total volume of the sample.

Table 6

Sample Name	Mercury Porosimeter			µCT at 16.1 µm Resolution		
	% Open Porosity	% Open Porosity at MPD	Mean Pore Diameter µm	% Open Porosity (µCT)	% Closed Porosity (µCT)	# of Layers Analyzed
2D A 1	37.61	19.12	16.4	16.36	0.23	976
2D B 1	18.15	9.83	16.4	10.97	0.72	765
2D B 2	17.71	3.49	16.4	2.76	2.23	742
3D A 1	10.65	2.25	16.4	2.73	0.60	1002
3D B 1	10.67	2.80	16.4	4.41	1.73	1310
CF 1	73.91	31.42	18.5	0.44	0.94	524
CF 3	67.22	1.59	16.4	0.69	3.84	722
CF 5	71.03	14.39	18.5	3.46	4.56	820
CF 7	34.11	0.93	16.4	1.59	0.97	648
Felt 1	44.11	25.59	17.2	19.80	0.19	2109
Felt 2	9.11	2.50	17.2	4.83	0.27	467
Felt 3	38.32	26.92	17.2	29.62	0.08	2167
Felt 4	10.57	2.46	17.2	5.28	0.25	2176
Felt 5	22.39	13.59	17.2	13.24	0.61	2041
Felt 6	11.19	6.96	17.2	5.84	0.67	2070
Felt 7	28.01	13.01	17.2	15.52	0.61	2065
Felt 8	12.11	5.98	17.2	8.63	2.05	2044
Felt 9	22.83	14.43	17.2	15.46	0.65	2055
Felt 10	20.74	12.26	17.2	18.99	0.53	2064
Felt 11	10.12	4.66	17.2	9.55	1.34	2062
Felt 12	20.26	10.77	16.4	8.99	1.44	2074
Felt 13	30.77	22.12	17.2	21.05	0.38	2121
Felt 14	36.68	22.96	17.2	18.23	0.54	2136
Felt 19	22.74	13.53	16.4	17.69	0.77	2155
Felt 20	24.90	15.07	16.4	18.08	0.69	2136
Felt 21	40.12	20.43	16.4	24.72	0.25	2106
Felt 22	34.08	21.26	16.4	19.90	0.37	2133
Felt 23	12.81	1.21	16.4	8.65	3.13	2156
Felt 26	10.10	1.35	16.4	0.69	9.42	2193
Felt 27	11.05	6.67	16.4	0.49	5.63	2092
Felt 28	18.10	12.64	16.4	7.12	1.35	2102
PPMC 1	16.27	2.13	16.4	4.80	1.34	1352
PPMC 2	23.75	5.55	16.4	7.95	0.73	1346
PPMC 3	25.73	10.25	16.4	9.84	0.56	1349
PPMC 4	18.14	3.65	16.4	8.64	0.88	1352
PPMC 5	21.86	6.35	16.4	5.01	1.31	1354
PPMC 6	21.17	6.77	16.4	5.38	0.95	1346
PPMC 7	18.92	7.41	16.4	5.56	1.04	1342

Table 7

Sample Name	Mercury Porosimeter		µCT at 8.0 µm Resolution		
	% Open Porosity at MPD	Mean Pore Diameter (µm)	% Open Porosity	% Closed Porosity	# of Layers Analyzed
2D A 1	22.14	8.2	23.37	0.43	1969
2D B 1	11.20	8.2	10.88	0.63	1531
2D B 2	6.02	8.2	7.05	0.62	1490
3D A 1	3.50	8.2	3.62	0.53	2015
3D B 1	3.39	8.2	4.18	1.74	2628
CF 1	38.73	8.1	2.42	5.39	1064
CF 3	35.08	8.0	2.78	7.93	1478
Felt 27	7.69	8.2	0.49	5.98	4173
Felt 28	13.09	8.0	12.11	0.10	4209
PPMC 1	5.26	8.2	4.02	0.93	2721
PPMC 2	10.23	8.2	10.29	0.58	2708
PPMC 3	12.56	8.2	16.03	0.99	2704
PPMC 4	7.73	8.2	6.59	0.73	2713
PPMC 5	8.42	8.2	9.92	1.05	2692
PPMC 6	8.27	8.2	11.41	1.75	2718

Table 8

Sample Name	Mercury Porosimeter		µCT at 4.0 µm Resolution		
	% Open Porosity at MPD	Mean Pore Diameter (µm)	% Open Porosity	% Closed Porosity	# of Layers Analyzed
3D A 1	4.74	4.1	8.03	1.10	4030
CF 3	63.12	4.1	19.37	0.83	2967

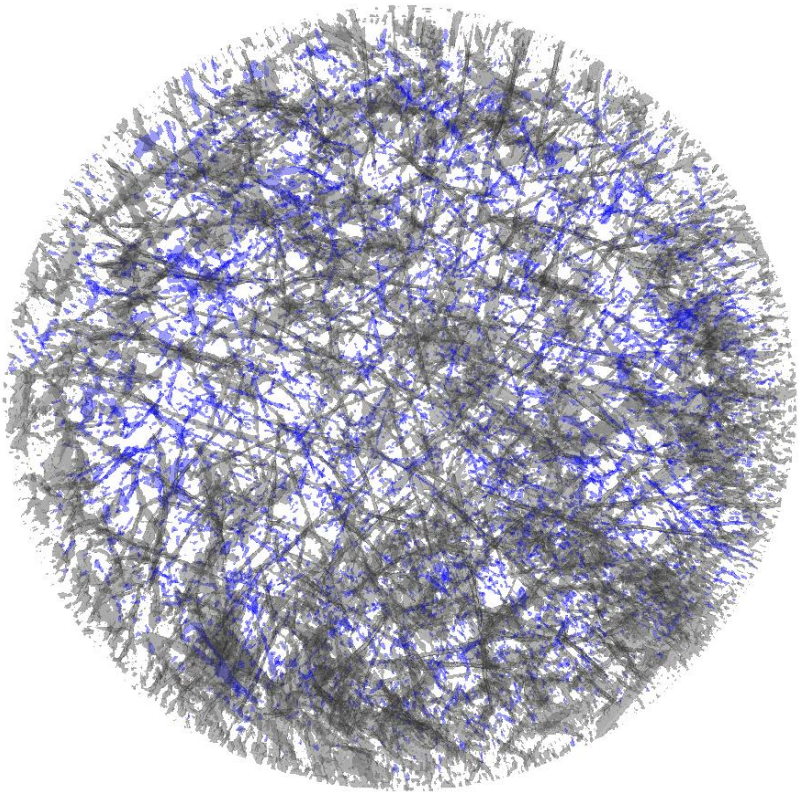

Figure 2

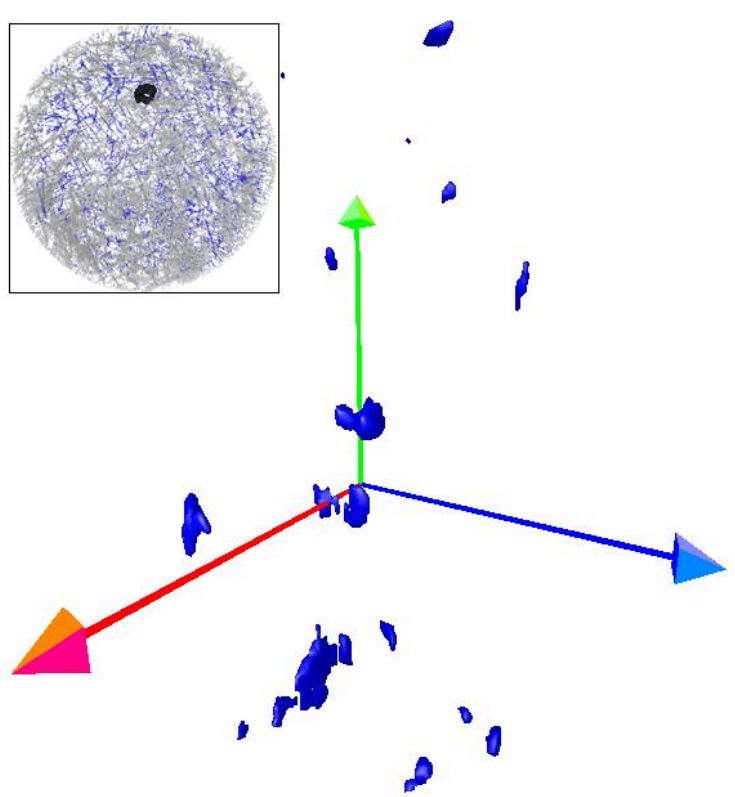

Figure 3

3.4 Closed Porosity

The μCT provides a nondestructive method for observing and determining the percent of closed porosity in a C-C composite. Although SANS [43] can quantify closed porosity in very small pores, this is currently the only method that is able to measure close porosity in this pore size range on a sample sized so that it is representative of the composite structure. The amount of closed porosity for each sample can be found in Table 6, Table 7, and Table 8 at resolutions of 16.1, 8.0, and 4.0 μm respectively. This technique and methodology allows one to determine how the different processing steps create closed porosity and limit the ability to densify a C-C composite. Throughout the analysis of all samples, a very small fraction of each sample was actually comprised of closed porosity. This can be seen in (Figure 2), where it is possible to see the amount, size, shape, and distribution of the closed and open porosity in the sample. In the past, it was only possible to get an estimate of the closed porosity by using equations involving the helium density, the bulk density, and the density of graphite (2.26 g/cm^3) [78].

3.5 μCT Sub-Pixel Effects

The main limitations of the μCT approach are the resolution and the sub-pixel effects. Ultimate pixel size of the Skyscan 1172A is ~1 μm, with a sample diameter of 4 mm. In this study, a sample diameter of 13.8 mm was chosen to give a sample representative of the entire composite. This sample diameter limited the resolution to 4 μm. Any porosity smaller than approximately three times larger than the scanning resolution cannot be detected due to sub-pixel effects. If the pores close to the scanning resolution are imaged, they may appear as noise and are probably filtered out during image processing.

Figure 2 illustrates a simple example of the sub-pixel effect. Figure 4a shows a pixel grid with the original feature, a circle. The circle has a diameter of about 2.5 pixels. Figure 4b shows how this circle would be depicted in a pixelized grayscale image. The grayscale image is then turned into a binary

image for analysis by choosing upper and lower threshold values for the image. By choosing a first set of threshold values, the area of the feature in Figure 4c has been reduced by 18% and the maximum dimension increased by 13%. In Figure 4d, another set of threshold values was chosen that significantly changed the features. As can be seen, the effects of both sub-pixels and threshold values can significantly alter the results.

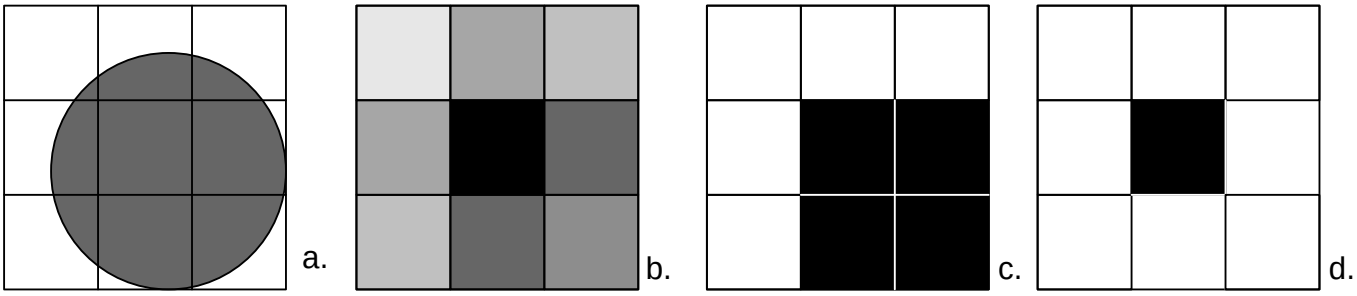

Figure 4

3.6 The value of multiple techniques

The results from Felt 27 are anomalous and they demonstrate the value of employing the porosimeter in conjunction with the μCT. The porosimeter results of sample Felt 27 (Table 6) show a porosity of about 11.05% with 6.67% open porosity at a MPD of 16.4 μm. In contrast, when looking at the 16.1 μm resolution μCT results, the open porosity is only 0.49% and the closed porosity is 5.63%. Comparing columns 3 and 5 in Table 6, one can see that the values measured by the porosimeter and μCT are usually rather close. In contrast, with sample Felt 27 the difference is more than an order of magnitude. Thus, this discrepancy in results appears real and studying it actually yields valuable insights that cannot be deduced by either technique separately. First, it should be noted that when the two μCT values are combined, the total porosity is close to the open porosity at that MPD for the porosimeter. A μCT slice near the middle of the sample can be seen in Figure 5. A large void in the center of the sample is obvious. The fact that the total porosity values measured by the two techniques is usually close as in

this case adds credence to the assumption that the different values are both correct and are dependent on what is being measured. That is, the porosimeter measures intrusion as a function of pressure. Thus, the large central void in Figure 5 will be characterized as having a minimum dimension equal to the minimum dimension of the pore(s) filling this central void. This effect is called bottlenecking and is difficult to prove without an additional visual technique. From Figure 6 it can be seen that there is a lot of porosity near 20 μm in diameter. Due to sub-pixel effects, these pathways to the porous central region are smaller than or close to the μCT scanning resolution and thus are not visible. Since they are not visible at this resolution, the porosity is characterized as closed porosity by the μCT. A similar situation exists with Sample Felt 26 as seen in Figure 1and Figure 7.

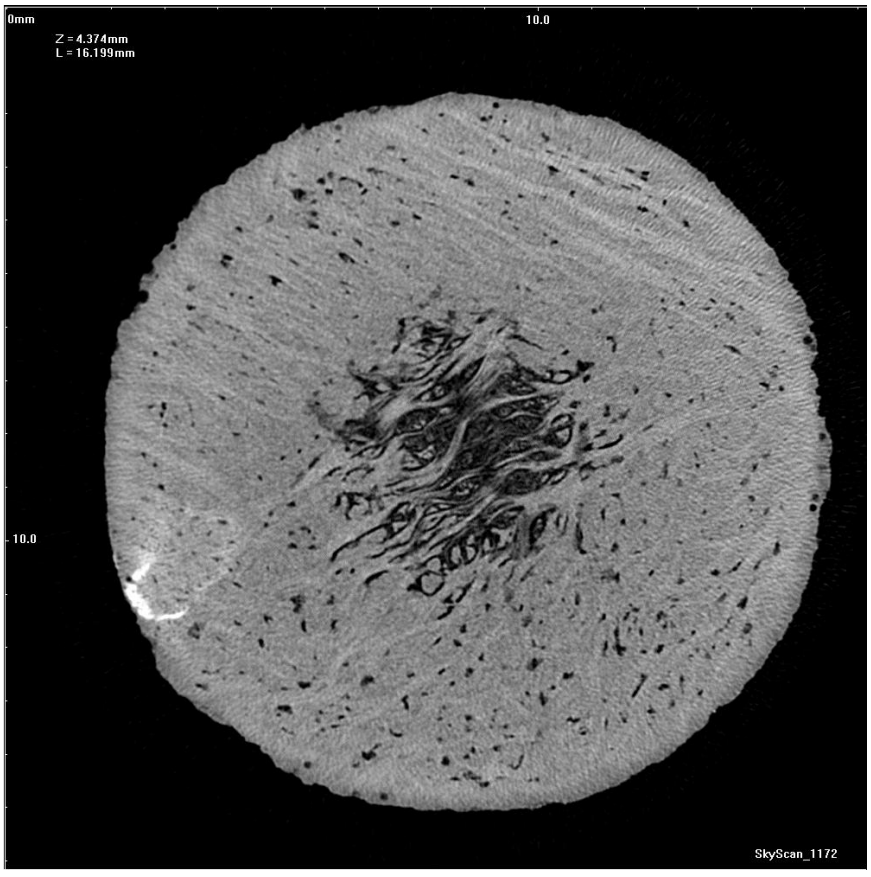

Figure 5

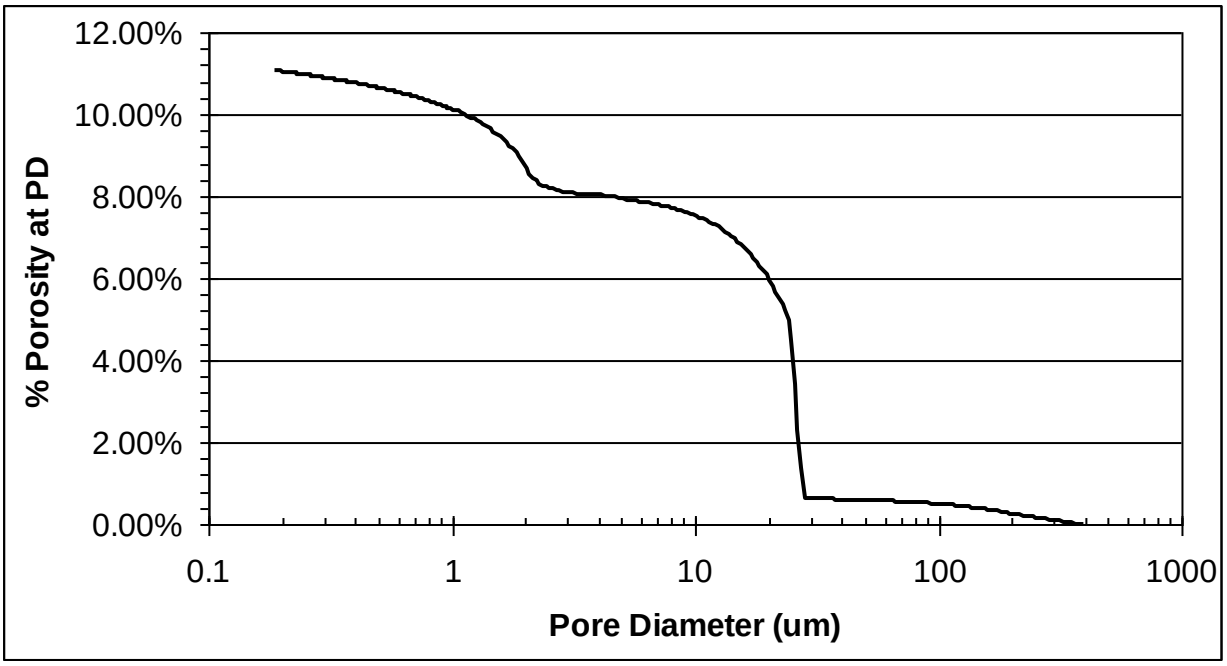

Figure 6

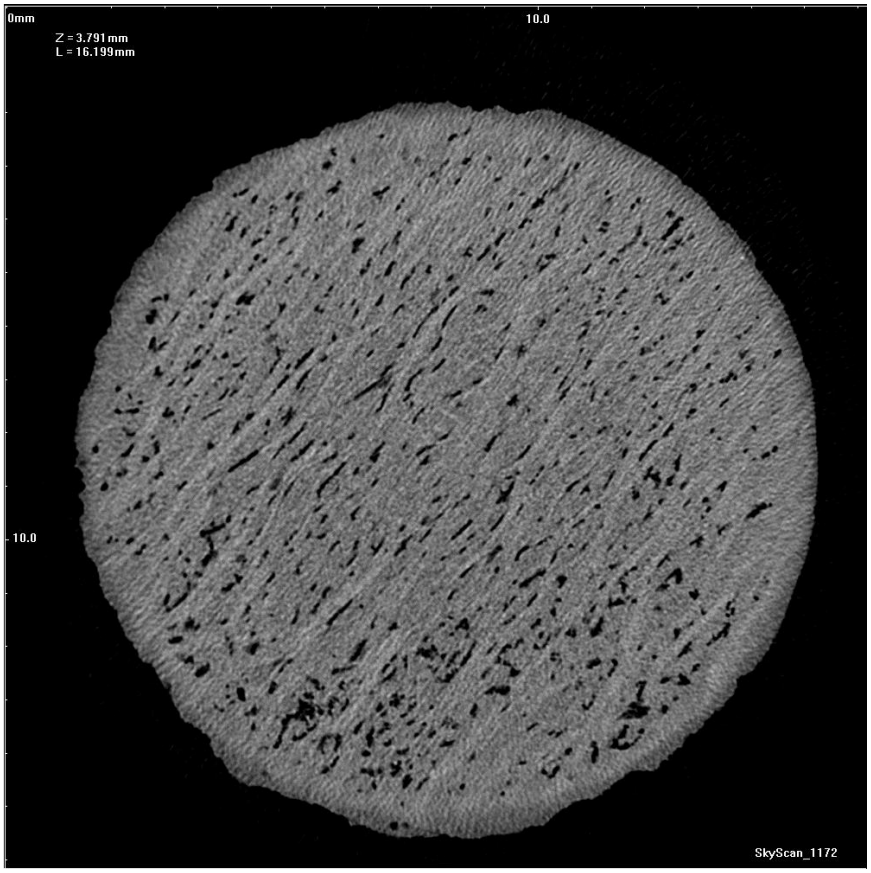

Figure 7

4. Conclusion

Apart from the sink-float method, the traditional methods for determining the skeletal density of C-C composites all provide results very close to one another. The new technique of μCT with proper analysis provides bulk density results that are close to those determined by the mercury porosimeter, which is the instrument most employed to characterize porosity distribution in carbonaceous materials. This is due to the fact that in addition to determining skeletal and bulk density, it is also able to provide quantitative information on pore size distribution. The μCT has additional advantages over the mercury porosimeter in that it provides quantitative information on not only density and porosity, but it provides this non-destructively and for larger samples. Also, it provides the ability to observe open- and closed-pore size, shape, and location in the sample in 3D for the first time. Finally, in conjunction with the porosimeter, micro-computed tomography is capable of identify the source of artifacts in the sample.

5. References

[1] Bansal RC, Donnet JP, Stoeckli F. Active Carbon. New York (NY): Marcel Decker; 1988. P. 119-62.

[2] Reid CR, Thomas KM. Adsorption of Gases on a Carbon Molecular Sieve Used for Air Separation: Linear Adsorptives as Probes for Kinetic Selectivity. Langmuir. 1999; 15(9):3206-18.

[3] Steel KM, Koros WJ. Investigation of porosity of carbon materials and related effects on gas separation properties. Carbon. 2003; 41(2):253-66.

[4] Centeno TA, Fernandez JA, Stoeckli F. Correlation between heats of immersion and limiting capacitances in porous carbons. Carbon. 2008; 46(7):1025-30.

[5] Ila D, Jenkins GM, Zimmerman RL, Evelyn AL. High porosity polymeric carbon ware for controlled release of drugs. Materials Research Society Symposium Proceedings. 1994; 331:281-5.

[6] Balik K, Sochor M, Pesakova V, Krena J, Glogar P, Gregor J. Carbon - carbon and carbon -polymer composite materials as components of implants for bone surgery. Acta Montana, Series AB: Geodynamics & Fuel, Carbon, Mineral Processing. 1999; 7(113):57-62.

[7] Zolkin PI, Tatarinov VF. Carbon endoprostheses and implants. Refractories and Industrial Ceramics. 1999; 40(3-4):150-1.

[8] Lozano-Castelló D, Alcañiz-Monge J, de la Casa-Lillo MA, Cazorla-Amorós D, Linares-Solano A. Advances in the study of methane storage in porous carbonaceous materials. Fuel. 2002; 81(14):1777–803.

[9] Jordá-Beneyto M, Suárez-García F, Lozano-Castelló D, Cazorla-Amorós D, Linares-Solano A. Hydrogen storage on chemically activated carbons and carbon nanomaterials at high pressures. Carbon 2007; 45(2):293–303.

[10] Nikitin YN. Role of the nature and structure of carbon black with high porosity and its interaction with matrixes in reinforcement of elastomers. Kauchuk i Rezina 2005; 4:18-20.

[11] Grelsson B. Correlations between porosity content, strength and ultrasonic attenuation in carbon fiber laminates. Materials & Design. 1992; 13(5):275-8.

[12] Huang J, Hao Z, Zou W, Liu J. Effect of microstructure on compressive strength of carbon prepared from coal tar pitch. Gongcheng Xuebao. 2007; 25(1):91-4.

[13] Rubin AM. The effect of porosity on the elastic constants of thin carbon fiber composite laminates. PhD [dissertation]. Saint Louis (MO): Washington University; 1993.

[14] Hosten B, Tittmann BR, Abdel-Gawad M. Elastic anisotropy of carbon - carbon composites during the fabrication processes. IEEE 1986 Ultrasonics Symposium. 1986. p. 1061-4.

[15] Krautwasser P, Balthesen E, Nickel H. Effect of microporosity on the irradiation behavior of pyrolytic carbon. Reaktortagung 1974; 6:436-9.

[16] Laine NR, Vastola FJ, Walker PL Jr. The importance of active surface area in the carbon-oxygen reaction. J Phys Chem. 1963; 67(10): 2030-4.

[17] Weng T-C, Teng H. Characterization of high porosity carbon electrodes derived from mesophase pitch for electric double-layer capacitors. J of the Electrochemical Society. 2001; 148(4):A368-73.

[18] Mirzaeian M, Hall PJ. Carbon electrode materials for Li/O2 batteries.Preprints of Symposia - American Chemical Society, Division of Fuel Chemistry. 2007; 52(2):695-9.

[19] Carmier D, Vix-Guterl C, Lahaye J. Porosity of the cathode during the discharge of SOCl2 /Li batteries I. Industrial cathodes. Carbon. 2001; 39(14):2181–6.

[20] El-Raghy SM, Williamson J, Samy TM, Ibrahiem MO. Porosity modifications in the carbon cathode of aluminum reduction cell. Light Metals; 2001; Warrendale, PA. 2001; p. 723-9.

[21] Muehlen H-J, van Heek KH. Porosity and thermal reactivity in carbonaceous materials. In: Patrick JW, editor. Porosity in Carbons : Characterization and Applications. New York : Halsted Press; 1995. p. 131-49.

[22] Rodriguez-Mirasol J, Thrower PA, Radovic LR. On the oxidation resistance of carbon - carbon composites: importance of fiber structure for composite reactivity. Carbon. 1995; 33(4):545-54.

[23] Zalameda JN. Measured through-the-thickness thermal diffusivity of carbon fiber reinforced composite materials. J of Comp Tech & Research 1999; 21(2):98-102.

[24] Slagtern, A.; Grjotheim, K.; Foosnaes, T.; Naterstad, T. Thermal expansion of carbon materials calcined at various temperatures: structure, pore volume and content of impurities. Light Metals; 1987; Warrendale, PA 1987; p. 449-57.

[25] Radovic LR, Rodriguez-Reinoso F. Carbon Materials in Catalysis In: Thrower PA, editor. Chemistry and physics of carbon A series of advances. Vol. 25. New York: Marcel Dekker; 1997. p. 243-358.

[26] Stoeckli F, Guillot A, Hugi-Cleary D, Slasli AM. Pore size distributions of active carbons assessed by different techniques. Carbon. 2000; 38(6):938-41.

[27] Pfeifer P, Ehrburger-Dolle F, Rieker TP, González MP, Hoffman WP, Molina-Sabio M, Rodríguez-Reinoso F, Schmidt PW, Voss DJ. Nearly Space-Filling Fractal Networks of Carbon Nanopores. Phys Rev Lets. 2002; 88(11):115502.

[28] Groszek AJ. Characterization of microporous carbons by flow microcalorimetry. Carbon. 1989; 27(1):33-9.

[29] Brun M, Lallemand A, Quinson J-F, Eyraud C. A new method for the simultaneous determination of the size and shape of pores: the thermoporometry. Thermochimica Acta. 1977; 21(1):59-88.

[31] Rodriguez-Reinoso F, Garrido J, Martin-Martinez JM, Molina-Sabio M, Torregrosa R. The combined use of different approaches in the characterization of microporous carbons. Carbon. 1989; 27(1):23-32.

[30] Gregg SJ, Singh KSW. Adsorption, surface area and porosity. London: Academic Press; 1982.

[32] Brunauer S, Emmett PH, Teller E. Adsorption of gases in multimolecular layers. J Am Chem Soc. 1938; 60(2):309-19.

[33] Masters KJ, McEnaney B. Structural analysis of microporous carbons using the Dubinin-Radushkevich equation. J Colloid and Interface Sci. 1983; 95(2);340-5.

[34] Spitzer Z, Bíba V, Kadlec O, The complete pore structure analysis of fine porous solids. Carbon. 1976; 14(3):151-6.

[35] Sing KSW. Overview of physical adsorption by carbons. In: Bottani E, Tascón J, editors. Adsorption by Carbons. Oxford (UK): Elsevier; 2008. p. 3-14.

[36] Stoeckli F, Guillot A, Slasli AM, Hugi-Cleary D. The comparison of experimental and calculated pore size distributions of activated carbons. Carbon. 2002; 40(3):383-8.

[37] Hoinkis E. Small Angle Scattering of Neutrons and X-Rays from Carbons and Graphites. Chemistry and Physics of Carbon. Vol. 25. New York (NY): Marcel Dekker; 1997. p. 71-242.

[38] Calo JM, Hall PJ. The application of small angle scattering techniques to porosity characterization in carbons. Carbon. 2004; 42(7):1299–1304.

[39] Foster MD, Jensen KF. SAXS investigation of model carbon pore structure and its change with gasification. Carbon. 1991; 29(2):271-82.

[40] Wang JI, Jenkins RG, Walker PL, Jr. Characterization of porosity in microporous carbons by small angle x-ray scattering. Extended Abstracts and Program - Biennial Conference on Carbon. 1979; 14:125-6.

[41] Mamun SM, Herstedt M, Oikawa K, Gustafsson T, Otomo T, Furusaka M, Kamiyama T, Sakaebe H, Edstrom K. Neutron - scattering studies on carbon anode materials used in lithium-ion batteries. Applied Physics A: Materials Science & Processing. 2002; 74 Suppl 2:S1028-30.

[42] Kieffer J. Investigation of the transitional pore structure of activated carbon fibers by small - angle neutron scattering. J Applied Phy. 1992; 72(12):5649-56.

[43] Calo JM, Hall PJ, Antxustegi M. Carbon porosity characterization via small angle neutron scattering. Colloids and Surfaces A: Physicochemical and Engineering Aspects. 2001;1 87-188:219-32.

[44] Endo M, Furuta T, Minoura F, Kim C, Oshida K, Dresselhaus G, Dresselhaus MS. Visualized observation of pores in activated carbon fibers by HRTEM and combined image processor. Supramolecular Science. 1998; 5(3-4):261-6.

[45] Kadlec O. On the theory of capillary condensation and mercury intrusion in determining carbon porosity. Carbon. 1989; 27(1):141-55.

[46] Ritter HL, Drake LC. Pressure porosimeter and determination of complete macropore-size distributions. Ind Eng Chem Anal Ed. 1945; 17(12):782-6.

[47] Lopata VJ, Roe L, Sidwell DR. Porosity measurements of advanced composites using mercury intrusion porosimetry - a new quality tool Materials Technology. 1999; 14(3):129-32.

[48] Zhou Y, Lentz H. Mercury porosimetry measures the volume of micropores in activated carbon. In: Keller JU, Reiner S, editors. Adsorption by porous solids: Festschrift in honor of Prof. Dr. sc.techn. Jürgen U. Keller. Düsseldorf: VDI-Verl; 1998. p. 34-46.

[49] Datta SK, Simhai N, Tewari AN, Gatica JE, Singh M. Permeability of microporous carbon preforms. Metallurgical and Materials Transactions A: Physical Metallurgy and Materials Science. 1996; 27A(11):3669-74.

[50] Klucakova M. Analysis of relationship between properties and behavior of materials used and impregnation conditions of carbon - carbon composites. Acta Materialia. 2005; 53(14):3841-8.

[51] Xu L-Y, Shi Z-G, Feng Y-Q. Preparation of a carbon monolith with bimodal perfusion pores. Microporous and Mesoporous Materials. 2008; 115(3):618-23.

[52] Dickinson JM, Shore JW. Observations concerning the determination of porosities in graphites. Carbon. 1968; 6(6):937-41.

[53] Pinoli PC, Johnson AC, Keller RL. Mercury porosimetry of 3-D carbon / carbon. Extended Abstracts and Program - Biennial Conference on Carbon. 1979; 14:243-4.

[54] Wang J, Qian J, Jin Z, Qiao G. Microstructure of C/C composites prepared by chemical vapor infiltration method with vaporized kerosene as a precursor. Materials Science & Engineering, A: Structural Materials: Properties, Microstructure and Processing. 2006; A419(1-2):162-7.

[55] Park HS, Choi WC, Kim KS. Process-microstructure relationships of carbon / carbon composites fabricated by isothermal chemical vapor infiltration. J Adv Mats. 1995; 26(4):34-40.

[56] Hoffman W, Fernandez MB, Rao MB. Characterization of porosity in nanoporous carbons. Carbon. 1994; 32(7): 1383-84

[57] More N, Basse-Cathalinat B, Baquey C, Lacroix F, Ducassou D. Application of novel techniques of medical imaging to the nondestructive analysis of carbon - carbon composite materials. Nuclear Instruments & Methods in Physics Research. 1983; 214(2-3):531-6.

[58] Maire E, Buffière JY, Salvo L, Blandin JJ, Ludwig W, Létang JM. On the Application of Microtomography in the Field of Materials Science. Advanced Eng Mats. 2001; 3(8):539-46.

[59] Kerckhofs G, Schrooten J, Van Cleynenbreugel T, Lomov SV, Wevers M. Validation of x-ray microfocus computed tomography as an imaging tool for porous structures. Review of Sci Instruments. 2008; 79(1):013711.

[60] Bugani S, Camaiti M, Morselli L, Van de Casteele E, Janssens K. Investigating morphological changes in treated vs. untreated stone building materials by x-ray micro-CT. Anal Bioanal Chem. 2008; 391(4):1343-50.

[61] Eckstorff F, Mohr C, Frohs W, Fendt F. X-ray tomography for the investigation of carbon and graphite materials. Carbon 2008; Nagano, Japan. Extended Abstract P0144.

[62] Babout L, Mummery PM, Marrow TJ, Tzelepi A, Withers PJ. The effect of thermal oxidation on polycrystalline graphite studied by x-ray tomography. Carbon. 2005; 43(4):765-74.

[63] Babout L, Mummery PM, Marrow TJ, Withers PJ. Mapping the evolution of density in 3D of thermally oxidized graphite for nuclear applications. Scripta Materiallia. 2006; 54(5):829-34.

[64] Douarche N, Rouby D, Peix G, Jouin JM. Relations between x-ray tomography, density and mechanical properties in carbon-carbon composites. Carbon. 2001; 39(10):1455-65.

[65] Berre C, Fok SL, Marsden BJ, Babout L, Hodgkins A, Marrow TJ, Mummery PM. Numerical modeling of the effects of porosity changes on the mechanical properties of nuclear graphite. J of nuclear materials. 2006; 352(1-3):1-5.

[66] Yen CL, Tittmann BR. Ultrasonic characterization of macroporosity. Proceedings of the American Society for Composites: 7th Technical Conference. 1992: 428-35.

[67] Shen Y, Ozzano C, Pietranera N, Mao C, Luzzato C, Rosatelli F, Williamson J. Application of ultrasonic inspection to carbon fiber composites in the manufacturing process. High Temperatures - High Pressures.1996; 27/28(3):299-305.

[68] Birt EA, Smith RA. A review of NDE methods for porosity measurement in fibre-reinforced polymer composites. Insight. 2004; 46(11):681-6.

[69] Delhaès P, Trinquecoste M, Lines J-F, Cosculluela A, Goyhénèche J-M, Couzi M. Chemical vapor infiltration of C/C composites: Fast densification processes and matrix characterizations. Carbon. 2005; 43(4):681–91.

[70] Granda M, Casal E, Bermejo J, Menéndez R. The influence of primary QI on the oxidation behaviour of pitch-based C/C composites. Carbon. 2001; 39(4):483–92.

[71] ASTM C830: Standard Test Methods for Apparent Porosity, Liquid Absorption, Apparent Specific Gravity, and Bulk Density of Refractory Shapes by Vacuum Pressure. West Conshohocken, PA; ASTM International; 2000 Revised 2006.

[72] ASTM C20: Standard Test Methods for Apparent Porosity, Water Absorption, Apparent Specific Gravity, and Bulk Density of Burned Refractory Brick and Shapes by Boiling Water. West Conshohocken, PA; ASTM International; 2000 Revised 2005.

[73] Canada DC, Laing WR. Use of a density gradient column to measure the density of microspheres. Anal Chem. 1967; 39(6):691-2.

[74] Miller PJ. Density gradient techniques in chemistry. Sch Sci Rev. 1971; 52(180):601-7.

[75] Lysenko SA, Zolkin PI, Platonova MV. Determination of the density of carbon fibers in a gradient column. Zavodskaya Laboratoriya. 1986; 52(6):60-1.

[76] Chioujones KM, Ho W, Chau PC, Fathollahi B, Wapner PG, Hoffman WP. Microstructural studies of In-Situ mesophase transformation in the fabrication of carbon-carbon composites. Carbon. 2006; 44(2):284-92.

[77] Feldkamp LA, Davis LC, Kress JW. Practical cone-beam algorithm. J Opt Soc Am A. 1984; 1(6):612-9.

[78] Biloe S, Mauran S. Gas flow through highly porous graphite matrices. Carbon. 2003; 41(3):525–37.

6. List of Caption of Figures and Tables

Figure 1: Felt 26 porosimeter cumulative graph showing the percent open porosity greater than or equal to a given mean pore diameter.

Figure 2: Open (grey) and closed (blue) porosity as seen looking down through 150 slices of the sample, PPMC 2.

Figure 3: 3D image of closed porosity from sample, PPMC 2, in dark enclosed volume of inset image.

Figure 4: Sub Pixel Effects. (a) pixel grid with original feature; (b) pixelized grayscale image; (c) result from first set of threshold values; (d) result from second set of threshold values.

Figure 5: μCT slice of Felt 27 showing uniform densification except for central void.

Figure 6: Felt 27 porosimeter cumulative graph showing the percent open porosity greater than or equal to a given mean pore diameter.

Figure 7: μCT of Felt 26

Table 1: Sample Information

Table 2 : μCT Processing Conditions

Table 3: Analysis Algorithm

Table 4: Skeletal Density (g/cm^3)

Table 5: Bulk Density (g/cm^3)